A calculation indicated that the total integrated power absorbed from the continuum was 5% of that absorbed from the Cu_L line.

In order to etch vertical-sidewall relief gratings into the substrate surface, reactive sputter etching was used. With this method, a directional or anisotropic etching is possible, and the problem of redeposition of material sputtered from the substrate surface is avoided. This latter problem is characteristic of ion beam etching (so-called ion milling) and rf sputter etching, and limits both the dimensional control and the sidewall angles that one can achieve.[12,13] The reactive sputter etching method is described in detail elsewhere.[14] In brief, we used a conventional rf sputter etching system at a frequency of 13.56 MHz and an rf power density of 0.3 W/cm^2. Etching was done in CHF_3 gas at a pressure of 10^{-2} Torr and a flow rate of 15 cm^3/min. Figure 2 illustrates sharp vertical-sidewall relief gratings etched into SiO_2. The groove widths are approximately 900 Å.

The material PMMA, such as in the resist pattern in Fig. 1, is etched at a rate of about 280 Å/min while SiO_2 is etched at a rate of about 200 Å/min. Thus, in order to etch vertical-sidewall grooves into the SiO_2, a more suitable mask is required. We used a chromium mask because it is etched at only about 12 Å/min, has a good adhesion, and is fine grained. The chromium grating was produced by the liftoff process using a resist pattern similar to that shown in Fig. 1, but where the PMMA was only 4200 Å thick.

We have demonstrated that soft x-ray lithography using Cu_L x radiation is an effective means of obtaining smooth-edged vertical-sidewall high-aspect-ratio relief gratings of 1600-Å linewidth in PMMA resist, and that such structures can also be etched into SiO_2 substrates by reactive sputter etching in CHF_3 gas. Application of such relief structures in SiO_2 will be discussed in a future publication.[3]

We would like to thank W. T. Brogan, M. Dalomba, P. D. DeGraff, N. Efremow, P. Phinney, G. Foley, and R. Reinhard for skillful technical assistance.

[1] J. I. Raffel and J. A. Yasaitis, IEEE Proc. 64, 1629—1630 (1976).
[2] H. Sakaki, K. Wagatsuma, J. Hamasaki, and S. Saito, Thin Solid Films 36, 497 (1976).
[3] D. C. Flanders and H. I. Smith, J. Vac. Sci. Technol. (to be published).
[4] A. N. Broers, W. W. Molzen, J. J. Cuomo, and N. D. Wittels, Appl. Phys. Lett. 29, 596 (1976).
[5] H. P. Zingsheim, *Scanning Electron Microscopy* 1977, Vol. I of *Proceedings, Workshop on Analytical Electron Microscopy*, edited by Om Johari (ITT Research Institute, Chicago, 1977), p. 357.
[6] R. J. Hawryluk, H. I. Smith, A. Soares, and A. M. Haryluk, J. Appl. Phys. 46, 2528—2537 (1975).
[7] H. I. Smith, Proc. IEEE 62, 1361 (1974).
[8] C. V. Shank and R. V. Schmidt, Appl. Phys. Lett. 23, 154—155 (1973).
[9] G. C. Bjorklund, S. E. Harris, and J. F. Young, Appl. Phys. Lett. 25, 451—452 (1974).
[10] R. Feder, E. Spiller, and J. Topalian, J. Vac. Sci. Technol. 12, 1332 (1975).
[11] D. C. Flanders and H. I. Smith, J. Vac. Sci. Technol. (to be published).
[12] H. I. Smith, *Proc. Symp. on Etching for Pattern Definition*, edited by H. G. Hughes and M. J. Rand (The Electrochemical Society, Princeton, 1976), p. 133.
[13] H. W. Lehmann, L. Krausbauer, and R. Widmer, J. Vac. Sci. Technol. 14, 281—284 (1977).
[14] H. W. Lehmann and R. Widmer, Appl. Phys. Lett. (to be published).

Hyperfine structure in the electronic spectrum of $^{127}I_2$ by saturated absorption spectroscopy at 633 nm

A. Morinaga and K. Tanaka

National Research Laboratory of Metrology, Tokyo, Japan
(Received 6 September 1977; accepted for publication 8 November 1977)

The full hyperfine components of the $R(127)$ line in the 11-5 band and the 10 components of the $P(33)$ line in the 6-3 band of the $B \leftarrow X$ electronic transition of $^{127}I_2$ were observed by the saturated absorption spectroscopy using a complex resonator He-Ne laser. The frequency of the laser was locked to each component and the frequency separations of the components were precisely measured. The hyperfine structure of the $R(127)$ line was compared with a model which included both a nuclear electric quadrupole and magnetic hyperfine interactions.

PACS numbers: 35.20.Sd, 42.55.Fn, 42.72.+h, 31.30.Gs

The hyperfine components of the $R(127)$ line in the 11-5 band of the $B\,^3\pi_{0u} + \leftarrow X\,^1\Sigma_g +$ electronic transition of $^{127}I_2$ are most important as visible wavelength standards and some of them are used as references for stabilizing a 633-nm He-Ne laser. Previously this hyperfine structure was investigated by Hanes *et al.*[1,2] by the method of saturated absorption spectroscopy using a He-Ne laser with an iodine cell in the resonator. They observed 14 components of the $R(127)$ line and the full components of the $P(33)$ line in the 6-3 band of the

 0003-6951/78/3202-0114$00.50

same electronic transition lying about 0.9 GHz to the red. However, the seven components in the lower-frequency region of the $R(127)$ line have not been identified because of the strong absorption by components of the $P(33)$ line in the same frequency region. In the present paper the full hyperfine components of the $R(127)$ line are identified by improving the signal-to-noise ratio.

In this study, for observing the hyperfine structure, a complex resonator He-Ne laser with a 10-cm-long iodine cell in the resonator, which can be tuned over a 1.5-GHz spectral range with a single-frequency oscillation, was used. This laser is composed of a 190-cm-long main resonator and a 10-cm-long folded path subresonator, which is used to select a single longitudinal mode.[3] The resonance frequency of the subresonator is modulated by vibrating a side mirror of the subresonator and is locked to the frequency of the laser output by the first-derivative locking technique so that the subresonator follows the main resonator. This complex resonator was constructed as stable as possible.[4] The maximum output power was about 10 mW without the iodine absorption cell and was reduced to a few mW with the iodine cell, whose temperature was stabilized to 10 °C.

The third-derivative signal of the laser intensity was used for the detection of the hyperfine components. This was obtained by synchronous detection of the third harmonics of the frequency-modulated laser intensity by vibrating the side mirror of the main resonator. By this detection, the signal-to-noise ratio was improved because of the elimination of the inclined background caused by the laser output curve. Figure 1 shows examples of the third-derivative signal of the laser intensity obtained by frequency scanning and shows the hyperfine components from a of the $R(127)$ line to g of the $P(33)$ line. The signal-to-noise ratio of the $R(127)$ line is about 5 and that of the $P(33)$ line is about 100. The components p and q of the $R(127)$ line can be resolved at a peak-to-peak modulation amplitude of 4 MHz, as shown in (A) in Fig. 1. The components s, t, and u of the $R(127)$ line are close to the components of the $P(33)$ line. The components s and t are at the lower-frequency side of the components e and f of the $P(33)$ line, as shown in (B). The component u is not observed, but we can estimate that the u component is hidden by the signal of component g of the $P(33)$ line.

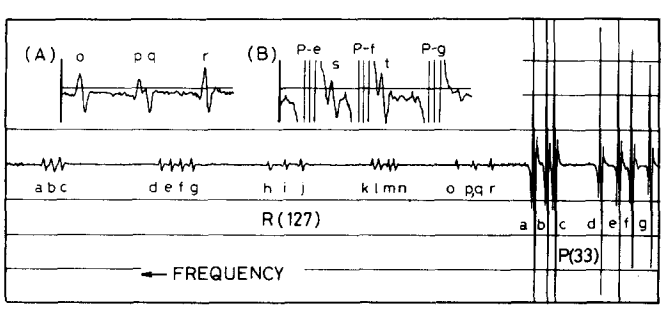

FIG. 1. Third-derivative signal of hyperfine components of $R(127)$ and $P(33)$ line of $^{127}I_2$, obtained at a peak-to-peak modulation amplitude of 6 MHz. (A) and (B) show enlarged views of the components o, p, g, r, s, and t of the $R(127)$ line, and e, f, and g of the $P(33)$ line. Both data were obtained at a peak-to peak modulation amplitude of 4 MHz.

TABLE I. Frequency separations of components of the $R(127)$ line relative to component i. Expt. and Calc. mean experimental and calculated results by the present work. (Unit: MHz.)

	F	Ref. 1	Ref. 5	Expt.	Calc.
a	$J+1$	297.3		299.8	299.8
b	J	288.5		291.0	291.1
c	$J-1$	280.7		282.9	283.1
d	$J+2$	166.9	165.13	165.1	165.1
e	$J+1$	153.6	152.27	152.2	152.3
f	$J-1$	139.7	138.91	138.9	138.9
g	$J-2$	126.3	125.71	125.6	125.9
h	$J+3$	22.3	21.96	22.1	22.0
i	J	0	0	0	0
j	$J-3$	−22.0	−21.56	−21.5	−21.3
k	$J+3$	−129.3		−129.9	−129.7
l	$J+2$	−137.1		−137.9	−137.7
m	$J-2$	−152.3		−153.8	−153.9
n	$J-3$	−162.0		−162.8	−162.7
o	$J+4$			−263.0	−262.8
p	$J+1$			−290.3	−290.0
q	$J-1$			−292.7	−293.0
r	$J-4$			−320.6	−320.5
s	$J+5$			−558.9	−558.5
t	J			−582.9	−583.0
u	$J-5$			−603 ~ −613	−607.7

To observe more components of the $P(33)$ line, the oscillating frequency region of the laser was expanded by lowering the temperature of the iodine cell to 0 °C. For this condition, the components from a to j of the $P(33)$ line were observed clearly; on the other hand, the components of the $R(127)$ line were hidden by noise because of very weak absorption.

Frequency separations between each hyperfine component and the i component of the $R(127)$ line were exactly measured by monitoring the beat spectrum of this laser and an iodine-stabilized He-Ne laser.[5] The frequency of the iodine-stabilized He-Ne laser was locked to the i component of the $R(127)$ line and that of the complex resonator laser was locked to the component from a of the $R(127)$ line to j of the $P(33)$ line step by step, except for components p, q, s, t, and u of the $R(127)$ line. The control system of the complex resonator laser is composed of the one used for the iodine-stabilized He-Ne laser and a subresonator control system. The oscillation frequencies of the two lasers were modulated at the same frequency, phase, and amplitude for minimizing the width of the beat spectrum. The beat signal was detected by an avalanche photodiode and its spectrum was observed by a spectrum analyzer with a superposed marker signal from a tunable oscillator, the frequency of which was measured by a frequency counter. As a result, the frequency separations of these components have been determined with an experimental error of ± 0.1 MHz. The frequency separations of the components p, q, s, and t of the $R(127)$ line from component i were determined with an experimental error of ± 0.5 MHz by interpolating the measured frequency separations by measuring their positions on the chart. The u component was supposed to be in the full width of the signal of the g component of the $P(33)$ line.

Table I shows the observed frequency separations

TABLE II. Frequency separations of components of the $P(33)$ line relative to component a. (Unit: MHz).

Comp.	Ref. 2	This work
a	0	0
b	−22.0	−22.0
c	−37.0	−36.8
d	−117.2	−118.2
e	−152.6	−153.9
f	−178.1	−179.2
g	−212.5	−214.5
h	−261.2	−263.5
i	−308.3	−310.2
j	−344.6	−347.3

of the hyperfine components of the $R(127)$ line with the values of the 14 components reported by Hanes *et al.*[1] and of the 7 components measured by Tanaka *et al.* with an accuracy of ±30 kHz.[5] Present results are in good agreement with the results by Tanaka *et al.* The frequency separations of 10 components of the $P(33)$ line relative to component a are given in Table II with the values for the equivalent components obtained by Hanes *et al.*[2] We consider that our result is more precise because of the beat frequency measurement. The frequency of component a of the $P(33)$ line was also found to be 393.5 ± 0.1 MHz lower than that of component i of the $R(127)$ line.

The hyperfine structure of the $R(127)$ line was explained as a combination of a nuclear electric quadrupole interaction and a magnetic hyperfine interaction by Kroll.[6] The authors also calculated the frequency separations of the $R(127)$ line by Kroll's model using the present values. The calculated frequency separations are given in column 6 of Table I and the total spins F of the upper and lower levels are assigned as shown in column 2. The overall agreement between the experimental and calculated values is within three times the experimental error. This small discrepancy will be reduced by the higher-order calculation.[7] The difference in nuclear electric quadrupole coupling constants for the ground and excited electronic states ΔeQq and the magnetic hyperfine coupling constant in the excited state K were determined as follows[8]:

$$\Delta eQq = -960.6 \pm 0.1 \text{ MHz},$$

$$K = 484.8 \pm 1.4 \text{ MHz}.$$

The obtained ΔeQq is consistent with the values calculated for the other hyperfine structures of the same electronic transition.[2,7,9,10]

[1]G.R. Hanes and C.E. Dahlstrom, Appl. Phys. Lett. **14**, 362 (1969).
[2]G.R. Hanes, J. Lapierre, P.R. Bunker, and K.C. Shotton, J. Mol. Spectrosc. **39**, 506 (1971).
[3]P.W. Smith, IEEE J. Quantum Electron. **QE-1**, 343 (1965).
[4]A. Morinaga and K. Tanaka, Jpn. J. Appl. Phys. **16**, 383 (1977).
[5]K. Tanaka, T. Sakurai, and T. Kurosawa, Jpn. J. Appl. Phys. **16**, 2071 (1977).
[6]M. Kroll, Phys. Rev. Lett. **23**, 631 (1969).
[7]P.R. Bunker and G.R. Hanes, Chem. Phys. Lett. **28**, 377 (1974).
[8]The notation ΔeQq and K are the same as in Ref. 6.
[9]L.A. Hackel, K.H. Casleton, S.G. Kukolich, and S. Ezekiel, Phys. Rev. Lett. **35**, 568 (1975).
[10]T.W. Hänsch, M.D. Levenson, and A.L. Schawlow, Phys. Rev. Lett. **26**, 946 (1971).

Eur. J. Phys. 18 (1997) 32–39. Printed in the UK PII: S0143-0807(97)74624-5

Laser-induced fluorescence of I_2 molecule in an undergraduate student laboratory

P Sikora, P Wiewiór, P Kowalczyk and C Radzewicz

Institute of Experimental Physics, Warsaw University, ul Hoża 69, 00-681 Warsaw, Poland

Received 20 May 1996, in final form 21 August 1996

Abstract. An experiment on laser-induced fluorescence of the iodine dimer is reported. The experiment, meant for an advanced undergraduate physics laboratory, requires relatively simple and inexpensive apparatus yet it introduces students to essential laser spectroscopy methods. Observation of the molecular spectrum demonstrates basic principles of quantum mechanics. Molecular parameters such as bond length, force constant, anharmonicity of the interatomic potential etc may be obtained from the analysis of the data. Finer phenomena, such as intensity distribution of spectral lines or collisional energy transfer between rotational levels, can also be studied. Apparatus, specific results and various stages of data analysis are described in the paper.

Streszczenie (In Polish). Przedstawiamy doświadczenie dotyczące badania widma cząsteczki I_2 przez obserwację fluorescencji wzbudzonej światłem laserowym. Doświadczenie to, przeznaczone dla pracowni dydaktycznych, zapoznaje studentów z metodami spektroskopii laserowej, mimo że wymaga stosunkowo prostej i taniej aparatury. Obserwowane widmo cząsteczkowe unaocznia podstawowe zasady mechaniki kwantowej. Analiza wyników doświadczenia pozwala wyznaczyć takie parametry cząsteczki jak długość wiązania, stała siłowa, anharmoniczność potencjału cząsteczkowego itd. Możliwa jest też obserwacja subtelniejszych zjawisk, takich jak rozkład natężeń linii widmowych lub zderzeniowy przekaz energii wzbudzenia między poziomami rotacyjnymi. Artykuł przedstawia układ doświadczalny, przykładowe wyniki pomiarów oraz kolejne etapy analizy otrzymanych rezultatów.

1. Introduction

Laser-induced fluorescence (LIF) of molecules is probably one of the most spectacular and colourful experiments in physics. At the same time, emission spectra originating from molecular levels selectively excited by laser light are relatively simple, yet provide a wealth of information about the structure of the molecules involved (e.g. bond lengths, force constants, interatomic potentials). Demand for experimentally determined molecular parameters coming from laser chemistry, plasma physics, astrophysics and other branches of science has brought about a renaissance of optical spectroscopy in the past decades.

We believe that it is particularly important to adapt experiments of contemporary significance to the undergraduate student laboratory, so that future physicists can become familiar with important phenomena and experimental techniques. Accordingly, we have designed a model experiment on LIF of the I_2 molecule, which includes basic elements of advanced laser spectroscopy research. Student experiments on the I_2 molecule, dealing with both absorption and emission spectra, have been already reported [1–3]. However, we propose several improvements leading to better accuracy and spectral resolution. This, in turn, allows for deeper analysis of the experimental data. The required apparatus is still reasonably simple, inexpensive and is probably available in many laboratories training physicists. The experiment is instructive from both a practical and theoretical point of view. It brings an advanced laboratory student into intimate contact with lasers, spectrometers, light detectors, lock-in techniques, computer data acquisition and analysis. On the other hand, the connection between the observed spectra and the structure of the molecule provides a rather simple and concrete example of quantum principles. The experimental results can be exploited in a variety of ways, from a mere observation of spectra and the underlying quantum rules to a lengthy analysis of the molecular structure. The student can pursue the analysis depending on his talent and temperament. We have found the experiment most effective in motivating deep and interesting questions concerning molecular and laser physics, at just the proper point in the student's career.

0143-0807/97/010032+08$19.50

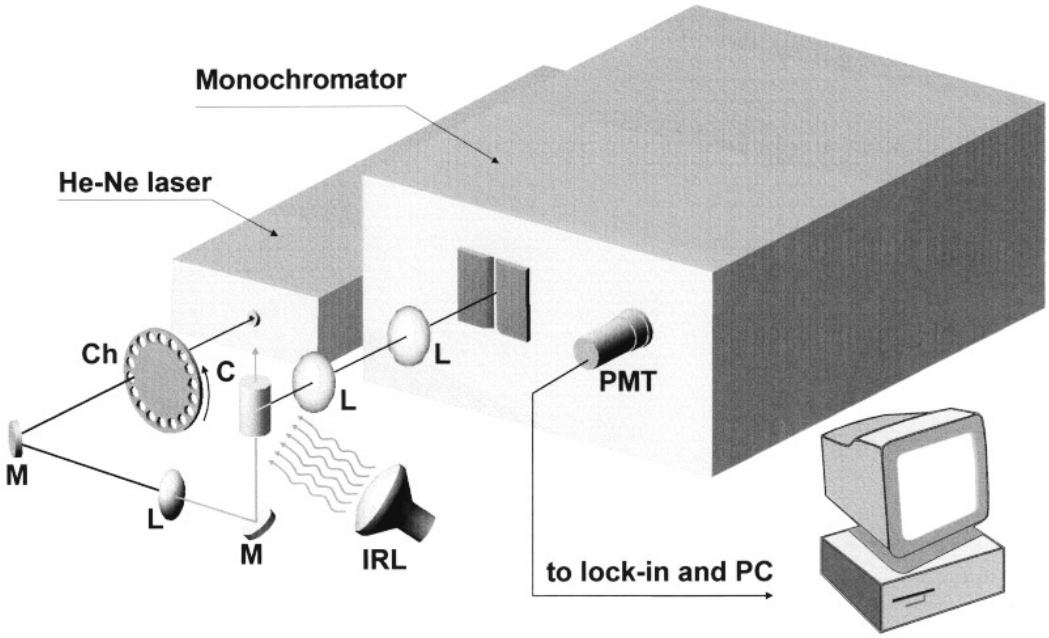

Figure 1. View of the experimental apparatus: C, iodine fluorescence cell; L, lenses; M, mirrors; IRL, infrared lamp; Ch, chopper; PMT, photomultiplier tube.

2. Experimental arrangement

Figure 1 presents the experimental setup. The fluorescence spectrum of the B–X system of I_2 (in a full spectroscopic notation: the B $0_u^+ - X\ ^1\Sigma_g^+$ system) is recorded photoelectrically in the region 11 500–17 000 cm^{-1} (figure 2). The fluorescence is excited by a beam from a He–Ne laser (Carl Zeiss, Jena) with a cavity length of 1.8 m, operating at 632.8 nm and providing up to 20 mW output power. The use of such a long cavity laser is clearly advantageous in this experiment. Small mode spacing in the laser spectrum causes several laser modes to overlap the Doppler broadened absorption line and this assures stable excitation. This cannot be achieved with a short cavity laser with a small number of modes which drift in or out of the absorption line profile. Therefore we recommend the use of a laser with a cavity length exceeding 3/4 m. The laser beam, chopped mechanically at frequency of about 200 Hz, is focused with $f = 50$ cm lens to about 100 μm diameter inside the iodine fluorescence cell made of a 5 cm diameter glass cylinder. It has been filled with a few crystals of iodine, evacuated to about 10^{-2} Torr using a simple rotary pump and then sealed off. It is highly advisable to use a liquid nitrogen trap when pumping out the cell in order to prevent contamination of the pump with iodine. The laser-induced molecular fluorescence of I_2 can be easily observed with a naked eye even at room temperature. The concentration of molecules and, consequently, the fluorescence intensity increase when the cell temperature is raised to about 60 °C. This can be done by blowing hot air from a commercial hairdryer. To avoid noise in our experiment we used an infrared lamp from a chicken incubator instead.

The molecular fluorescence was imaged with two glass lenses ($f = 12$ cm) onto an entrance slit of a 1.1 m grating double monochromator GDM-2 (Carl Zeiss, Jena) with two 600 grooves/mm plane reflectance gratings blazed at 500 nm. When operated with 100–150 μm slits the monochromator provided resolution of about 2 cm^{-1} in the first order of the gratings (compared to the Doppler width of molecular lines equal to approximately 0.01 cm^{-1}). This was quite sufficient to resolve all but a few lines in the I_2 fluorescence spectrum (figure 3). The use of a double monochromator is not essential since the amount of laser light scattered on the cell walls is quite low. Thus similar results could be obtained with any monochromator with comparable resolution; we used a double monochromator simply because it was available. The monochromator was equipped with an absolute angle encoder measuring the wavenumber in 0.1 cm^{-1} steps. A photomultiplier tube with a multi-alkali photocathode was used as a light detector behind the monochromator. A signal from the photomultiplier was measured with a lock-in amplifier (Ithaco model 3981) and recorded in a PC together with the wavenumber information. A computer code written by a student read the data from the angle encoder, controlled the lock-in amplifier and recorded the spectra.

The monochromator was calibrated with about 25 argon lines from a Plücker discharge tube, covering

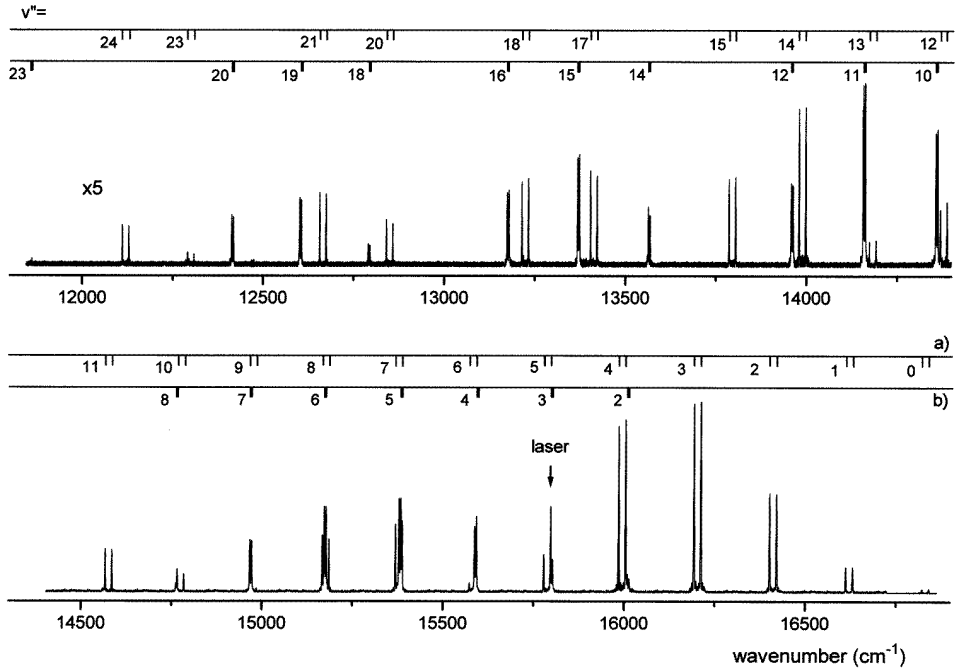

Figure 2. Fluorescence spectrum of I_2 excited by the 632.8 nm line from the He–Ne laser (the laser frequency is indicated by an arrow). The relative intensities have not been corrected for the spectral response of the photomultiplier and the monochromator. The assigned vibrational progressions correspond to (a) $(v' = 11, J' = 128) \rightarrow (v'', J'' = 127, 129)$ and (b) $(v' = 6, J' = 32) \rightarrow (v'', J'' = 31, 33)$ transitions.

in a uniform way the whole spectral region of interest. The calibration procedure is an indispensable part of the experiment allowing the student to get acquainted with standard spectral line tables and the procedure itself.

3. Experimental results and discussion

The discussion included in this section is intended only to aid the reader in understanding the experimental results. Some crucial details are presented in the appendices. Much more comprehensive presentations of the theory of molecular spectra and structure are available in the literature [4–7].

3.1. Observed LIF spectrum

The LIF spectrum observed in the experiment is displayed in figure 2. When iodine vapour is illuminated with monochromatic light from the He–Ne laser the only levels excited are those whose energy of excitation above one of the low-lying molecular levels populated in the gas sample coincides with the frequency of the laser line within the limits of Doppler broadening. It has been experimentally verified [8] that the 632.8 nm laser line excites in this way two transitions in the B–X band system of I_2, namely $(v' = 6, J' = 32) \leftarrow (v'' = 3, J'' = 33)$ and $(v' = 11, J' = 128) \leftarrow (v'' = 5, J'' = 127)$. Note that in the spectroscopic notation primes denote the upper level and double primes the lower level in the transition; also the higher energy state precedes the state of lower energy. In the fluorescence from the two excited levels $(v' = 6, J' = 32)$ and $(v' = 11, J' = 128)$ of the B state back to the electronic ground state levels any change Δv in the vibrational quantum number is permitted. On the other hand, the fluorescence transitions should conform to the fundamental selection rule $\Delta J = 0, \pm 1$, which results from conservation of angular momentum in a molecule + photon system. However, since the B–X band is of $^1\Sigma$–$^1\Sigma$ type, ΔJ values are restricted to J'–$J'' = -1$ (so called P lines) and J'–$J'' = +1$ (R lines). An explanation of this restriction, reaching deeply into the symmetry properties of wavefunctions of molecular states involved in the transition, is given in appendix I. Accordingly, in the experimental fluorescence spectrum we observe two series of doublets, each consisting of P and R lines (see figure 2). The fluorescence series form vibrational progressions, corresponding to transitions from a given laser excited (v', J') level in the B state to subsequent $(v'' = 0, 1, 2 \ldots, J'' = J' \pm 1)$ levels in the ground X state. The series are easy to distinguish. They originate from levels with very different values of J' and the P–R distance differs approximately by a factor of four (see next section for details). Both series meet at the laser frequency (though excitation proceeds via P line in one and via R line in the other) and diverge far from the laser line. The vibrational assignment is

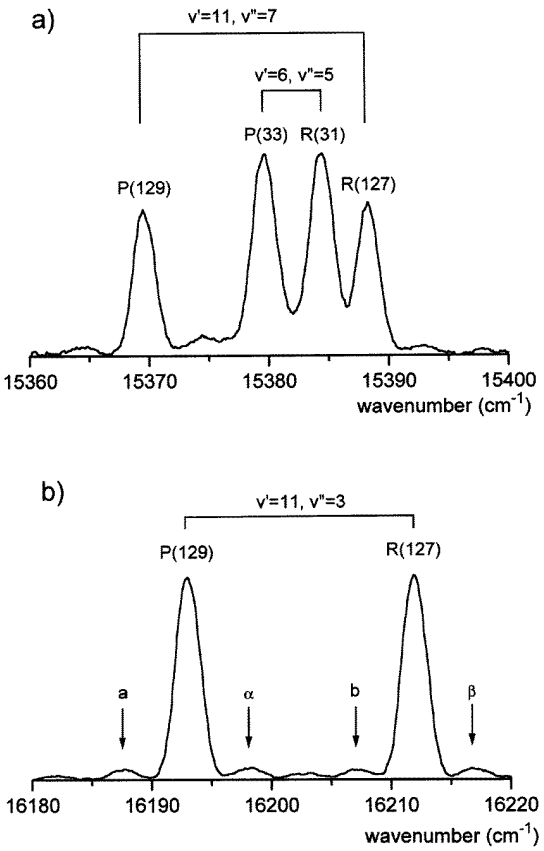

Figure 3. Fragments of figure 2, showing in detail (a) the $(v' = 6, J' = 32) \rightarrow (v'' = 5, J'' = 31, 33)$ and $(v' = 11, J' = 128) \rightarrow (v'' = 7, J'' = 127, 129)$ fluorescence lines; (b) the $(v' = 11, J' = 128) \rightarrow (v'' = 3, J'' = 127, 129)$ lines augmented by molecular fluorescence from collisonally populated levels: $(v' = 11, J' = 130)$—lines denoted as a and b, and $(v' = 11, J' = 126)$—lines denoted as α and β.

straightforward as we know levels excited by the He–Ne laser. In fact this information is redundant for the progression originating from the $(v' = 11, J' = 128)$ level where doublets with measurable intensity begin from $v'' = 0$ (and extend to $v'' = 24$ in our experiment). For the series from the $(v' = 6, J' = 32)$ level a direct assignment of v'' is not possible: fluorescence lines to vibrational levels $v'' = 0$–2 are too weak to be observed and the recorded doublets span only $v'' = 3$–23 range.

3.2. Determination of the molecular constants for the $X\ ^1\Sigma_g^+$ state

The observed fluorescence spectrum of the $B\ 0_u^+ \rightarrow X\ ^1\Sigma_g^+$ transition can be used to determine molecular constants describing the ground electronic state of the I_2 molecule.

The total energy of the molecule in a given state is well approximated by a sum of three components

$$E_{\text{total}} = E_{\text{el}} + E_{\text{vib}} + E_{\text{rot}}. \tag{1}$$

E_{el} is the electronic energy at the minimum of the potential well, E_{vib} is the energy of molecular vibration and E_{rot} is the rotational energy. Modelling the molecule as an anharmonic oscillator, we may write

$$E_{\text{vib}} = \omega_e(v + 0.5) - \omega_e x_e(v + 0.5)^2 \tag{2}$$

where for the values of the molecular constants a relation $\omega_e \gg \omega_e x_e$ holds. (A simple argument for the deviation from harmonic vibration is Coulomb repulsion of the two nuclei, as a result of which the internuclear distance can increase more readily than decrease and thus Hooke's law is not strictly obeyed.) The vibrational constant ω_e, when measured in cm^{-1} (a wavenumber unit of widespread use in spectroscopy), can be expressed as $\frac{1}{2\pi c}\sqrt{\frac{k}{\mu}}$ with μ being the reduced mass of the molecule, k the force constant and c the velocity of light. For molecular rotation a non-rigid rotator model is appropriate, i.e. that of two point masses connected by a spring. The rotational energy is in this case

$$E_{\text{rot}} = BJ(J + 1) - DJ^2(J + 1)^2 \tag{3}$$

with $B \gg D$. The rotational constant B (in cm^{-1}) equals to $h/8\pi^2 c\mu R_e^2$ where h is the Planck constant and R_e denotes the equilibrium length of the molecular 'spring', i.e. the equilibrium distance of the nuclei. The second term in (3), correcting the well known formula for the energy of a rigid rotator, expresses the action of centrifugal force on the rotating molecule. It causes the internuclear distance to increase with increasing rotation and diminishes the rotational energy. Finally, we have to take into account that rotation and vibration take place simultaneously and can influence each other. In the simplest model the rotational constant B acquires a v-dependence of the form:

$$B = B_e - \alpha_e(v + 0.5). \tag{4}$$

A similar expression holds for the centrifugal distortion constant D. However, as the v-dependent term is very small in this case, we may approximate simply $D = \text{constant}$ and denote it as D_e.

Consequently, we describe the $X\ ^1\Sigma_g^+$ state of I_2 using five molecular parameters: ω_e, $\omega_e x_e$, B_e, D_e and α_e (note that for the ground state we choose $E_{\text{el}} = 0$). These parameters can be obtained from the measured fluorescence spectrum in the following way. The line positions $\nu(v', J' \rightarrow v'', J'')$ of a fluorescence series represent the difference between the upper state energy $E'(v', J')$ (fixed for a given series) and the energy of the (v'', J'') ground state level:

$$\begin{aligned}\nu(v', J' \rightarrow v'', J'') = {} & E' - \omega_e(v'' + 0.5) \\ & + \omega_e x_e(v'' + 0.5)^2 - B_e J''(J'' + 1) \\ & + D_e J''^2(J'' + 1)^2 + \alpha_e(v'' + 0.5)J''(J'' + 1).\end{aligned} \tag{5}$$

In the first step of the analysis we must note that the spacing between the two doublet members $(v', J') \rightarrow$

Table 1. Molecular constants for the $X\ ^1\Sigma_g^+$ state of I_2 (all in cm^{-1}) determined in this experiment, compared to the best literature values. We treat results from [9] as 'exact' ones as their precision exceeds ours by several orders of magnitude.

	This experiment	[9]
ω_e	214.54 ± 0.10	214.5292
$\omega_e x_e$	0.63 ± 0.01	0.6130
B_e	0.0375 ± 0.0005	0.037 368
D_e	$(7 \pm 4) \times 10^{-9}$	4.5354×10^{-9}
α_e	$(1.24 \pm 0.10) \times 10^{-4}$	1.1382×10^{-4}

$(v'', J'' = J' + 1)$ and $(v', J') \rightarrow (v'', J'' = J' - 1)$ of the P–R fluorescence series equals

$$\Delta\nu_{rot} = 4(J' + 0.5)[B_e - 1.5D_e - 2D_e(J' + 0.5)^2 - \alpha_e(v'' + 0.5)]. \quad (6)$$

Plotting $\Delta\nu_{rot}/4(J' + 0.5)$ against $(v'' + 0.5)$ for each of the two fluorescence series separately, we can determine the constants B_e, D_e and α_e.

To find the other two molecular constants, ω_e and $\omega_e x_e$, we have to consider spacings between pairs of lines $(v', J') \rightarrow (v'', J'')$ and $(v', J') \rightarrow (v'' + 1, J'')$ of the same fluorescence progression, given by

$$\Delta\nu_{vib} = \omega_e - \alpha_e J''(J'' + 1) - \omega_e x_e(v'' + 1). \quad (7)$$

With the α_e value determined before, from the plot of $\Delta\nu_{vib}$ against $(v'' + 1)$ the two remaining vibrational constants can be determined.

The molecular constants calculated from the experimental spectrum shown in figure 2 agree within experimental error with the highly accurate values obtained for I_2 by Fourier transform spectroscopy [9] (see table 1). The precision of our experiment is sufficient to determine the vibrational constant to 0.05% [sic!], the anharmonicity to 1.5% and the rotational constant to 1.3%. For the two other molecular parameters we get rather an order of magnitude estimate.

The molecular constants can be used to calculate physical quantities of a more direct, 'classical' meaning. One has to remember, of course, that they are not always to be taken literally. For example, for a quantum oscillator even in the lowest state ($v = 0$) its position can be predicted only as a Gaussian distribution of probability—in contrast to a motionless classical oscillator resting at the equilibrium position. Nevertheless, we found that calculating the 'classical' parameters is appealing to the students and helps them to get a feeling about the phenomena involved. Thus from the rotational constant $B_e = 0.0375\ cm^{-1}$ we get, using $\mu = 1.05 \times 10^{-25}$ kg [10], the separation of two iodine nuclei $R_e = 2.66$ Å. This value can be compared to the mean radius of the valence 5p orbital in a free iodine atom, $\langle r \rangle = 1.32$ Å [10]. R_e is nearly exactly equal to $2\langle r \rangle$; this helps to visualize the extent of overlap of atomic orbitals in the ground molecular state. The frequencies of rotation in the $J = 1, 2, 3 \ldots$ states are $f_{rot} = 2cB_e\sqrt{J(J+1)} = 3.2$, 5.5 and $7.8 \times 10^9\ s^{-1}$, respectively (see appendix II for a simple derivation of the above formula), which corresponds to rotation periods of order of 10^{-10} s = 100 ps. We can compare these numbers to the vibrational frequency $f_{vib} = c\omega_e = 6.4 \times 10^{12}\ s^{-1}$ and vibrational period 1.5×10^{-13} s = 0.15 ps. Thus the period of molecular rotation turns out to be greater than the period of oscillation by few orders of magnitude. This could be expected from the hierarchy of molecular energies: the rotational levels are usually much more densely spaced than the vibrational levels. From the vibrational frequency and the reduced mass of the molecule we can evaluate the force constant $k = 1.7 \times 10^2\ N\ m^{-1}$. Surprisingly, this is about the same force constant as for a kitchen spring balance, with a spring stretching by 5 cm under 1 kg weight. But from our everyday experience the vibrational frequency of the balance may be of order of few Hz only. It is mass of the atoms which makes the difference!

3.3. Intensities of the fluorescence lines

The absolute intensities of I_2 fluorescence lines are difficult to measure as it would require precise calibration of the spectral response of our optical system. In particular, in the 590–850 nm spectral range covered in the experiment, the quantum efficiency of our photomultiplier tube changes dramatically. However, we would like to comment on a feature of the spectrum which can be recognized even without calibration, namely why some lines in a fluorescence progression are strong whereas others cannot be observed at all.

The observed fluorescence intensity for a transition from a fixed upper state level (v', J') to the ground state levels (v'', J'') is proportional to the population of excited molecules and the spontaneous emission coefficient $A(v'J' \rightarrow v'', J'')$ for the transition. The ratio of intensities for two members of the same fluorescence series is given by

$$\frac{I_1}{I_2} = \frac{A(v', J' \rightarrow v_1'', J'')}{A(v', J' \rightarrow v_2'', J'')}. \quad (8)$$

With the molecular wavefunction factorized according to (AI.1) and assuming that the electronic transition moment [4] does not depend on the internuclear distance, the fluorescence intensity ratio may be rewritten as

$$\frac{I_1}{I_2} = \frac{\nu^3(v', J' \rightarrow v_1'', J'')FC(v', v_1'')}{\nu^3(v', J' \rightarrow v_2'', J'')FC(v', v_2'')}. \quad (9)$$

Here ν is the frequency of the transition and $FC(v', v'')$ is the Franck–Condon factor for the transition defined as the square of the vibrational overlap integral

$$FC(v', v'') = \left| \int \psi_{vib}(v')\psi_{vib}(v'')\,dR \right|^2 \quad (10)$$

where $\psi_{vib}(v')$ and $\psi_{vib}(v'')$ are the upper and lower state vibrational wavefunctions.

Now we shall restrict our analysis to a specific problem: why the $(v' = 6, J' = 32) \rightarrow (v'' =$

5, $J'' = 31, 33$) lines are so strong, whereas the ($v' = 6, J' = 32$) $\rightarrow$ ($v'' = 9, J'' = 31, 33$) lines are missing from the spectrum (cf figure 2)? Since the frequencies in equation (9) are very close, the answer must follow from the values of the Franck–Condon factors for both transitions. Calculation of exact wavefunctions for the anharmonic potential, assumed for I_2 in this work, is rather a formidable task for a student. However, we can get qualitatively correct results by using a much simpler harmonic oscillator model. The vibrational wavefunctions are given in this case by analytical formulae (see appendix III). Even then the integrals (10) are much easier to calculate numerically. The necessary parameters for the X state wavefunction have been determined in section 3.2. For the B state we have to use the literature values $\omega_e = 125.67$ cm^{-1} and $R_e = 3.027$ Å [9]. The results turn out to be quite instructive. Figure 4 shows the wavefunctions, their products and the accumulated integrals for both transitions under consideration. Note that the equilibrium distances for both electronic states are much different and the vibrational wavefunctions occupy quite different regions in the R-space. For the ($v' = 6$) $\rightarrow$ ($v'' = 5$) transition the wavefunctions are in phase in the region of overlap and it is clear that the integral accumulates in this region to a high value. For the ($v' = 6$) $\rightarrow$ ($v'' = 9$) transition the wavefunctions are clearly out of phase. Therefore their product changes sign several times and the contributions to the integral cancel, giving the net value close to zero. The ratio of the Franck–Condon factors obtained from this simple model is about 190, accounting well for the absence of the ($v' = 6$) $\rightarrow$ ($v'' = 9$) lines in the experimental spectrum.

3.4. Inelastic collisions of excited molecules

A close inspection of the experimental spectrum reveals that the resonance fluorescence series are augmented by additional weaker emission lines (see figure 3(b)). These lines are due to iodine molecules losing or gaining rotational energy in inelastic collisions with surrounding atoms or molecules. The collisions lead to the population of levels other than those directly excited by the laser light and consequently to fluorescence from these levels. It can be easily observed that the 'extra' fluorescence originates from the B state levels lying close to the laser excited (v', J') levels. Such transitions are clearly seen around ($v' = 11, J' = 128$) $\rightarrow$ (v', J'') fluorescence series (figure 3(b)) where high rotational number allows the resolution of closely spaced spectral features. In this case we observe weak P and R lines originating from the ($v' = 11, J' = 128 \pm 2n$) levels where $n = 1, 2, \ldots$. The selection rule $\Delta J = \pm 2n$ in collisions is based on symmetry properties of molecular levels and reflects the basic rule that the nuclear spin states are not affected by collisions. A somewhat more detailed discussion is given in the appendix IV. It is interesting to note that the first experimental observation of this rule dates from far before the laser age and was accomplished in the same B–X system of I_2 [11].

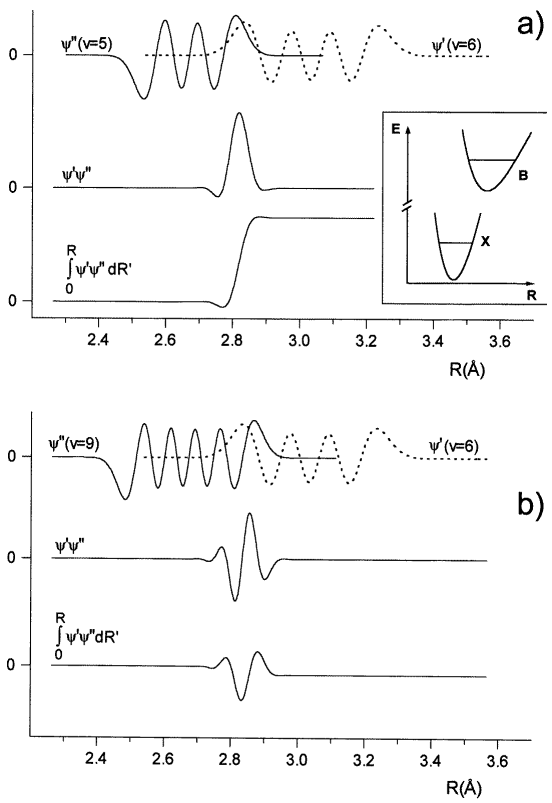

Figure 4. Vibrational wavefunctions, their products and the accumulated overlap integrals for the B $0_u^+ \rightarrow$ X $^1\Sigma_g^+$ transitions discussed in the text: (a) ($v' = 6$) $\rightarrow$ ($v'' = 5$) and (b) ($v' = 6$) $\rightarrow$ ($v'' = 9$).

4. Concluding remarks

So far, the model LIF experiment on I_2 has been carried out at Warsaw University by approximately twenty pairs of students. The standard analysis consisted of the determination of molecular parameters; better students have been encouraged to explore finer details of the experimental results. Operating the laser, monochromator and detection system has proved to be well within the capability of senior undergraduates. On the average we have allowed 4 four-hour sessions for the experimental part followed by data analysis done by students by themselves.

Appendix I

The ground molecular state of I_2 is customarily labelled as X $^1\Sigma_g^+$. Σ means here that the orbital angular momentum of the electrons is equal to zero; the superscript 1 is the spin multiplicity of the state written as $2S+1$ where S refers to the total spin of the electrons ($S = 0$ here): $+$ and g signs refer to the symmetries of the molecular wavefunction [4–7]. The excited B state

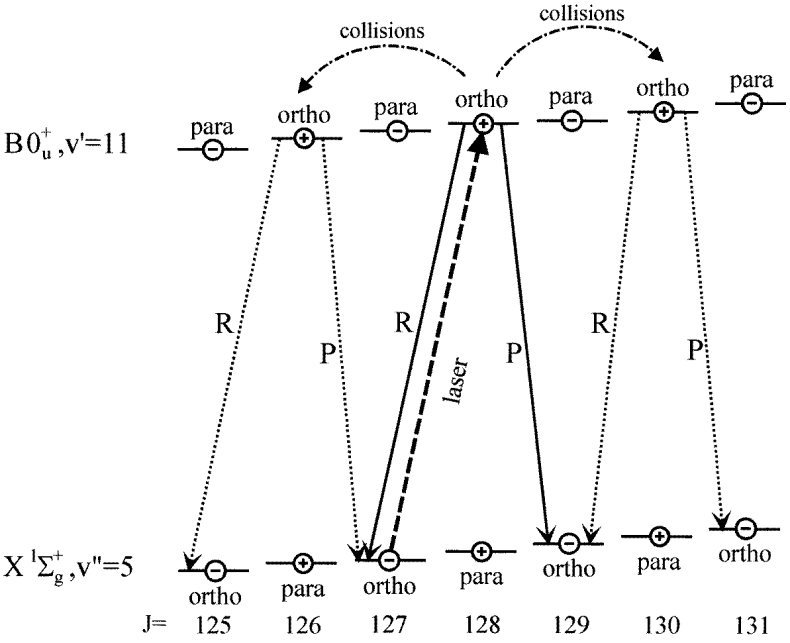

Figure 5. Symmetries of levels and exemplary allowed rotational transitions in the B $0_u^+ \rightarrow$ X $^1\Sigma_g^+$ system of I_2 after laser excitation of the $(v' = 11, J' = 128)$ level in the B state. The collisional energy transfer and following fluorescence are also shown.

can be described properly rather in a so-called Hund's coupling case (c) as 0_u^+; however, its level structure and symmetry properties are identical to that of a $^1\Sigma_u^+$ state. (Understanding of Hund's case (a) $\rightarrow$ (c) transition is a challenge for ambitious students.) To explain the B $\rightarrow$ X fluorescence spectrum, we must discuss in some detail symmetries of molecular levels and selection rules governing radiative transitions between them.

The total wavefunction of a molecule on a given energy level is, to a first approximation, a product of an electronic, vibrational, rotational and nuclear wavefunctions

$$\psi_{\text{total}} = \psi_{\text{el}} \cdot \psi_{\text{vib}} \cdot \psi_{\text{rot}} \cdot \psi_{\text{nucl}} \qquad \text{(AI.1)}$$

where the first three functions depend on coordinates of the electrons and nuclei (hence their product is often referred to as a coordinate function) and the last one on orientation of nuclear spins. The molecular levels are classified as positive (+) or negative (−) according to the behaviour of the coordinate wavefunction when the laboratory coordinate system is inverted about the origin (i.e. when for all particles composing the molecule x is replaced by $-x$, y by $-y$ and z by $-z$): for positive levels the wavefunction remains unchanged and for negative ones it changes the sign. Each of the three factors in the coordinate wavefunction behaves in a well-defined way. Inversion always leaves the vibrational wavefunction ψ_{vib} unaltered since it depends only on the magnitude of the internuclear distance. For the simplest model of a rigid rotator, whose wavefunctions are spherical harmonics, ψ_{rot} remains unchanged for even values of the J quantum number but changes to $-\psi_{\text{rot}}$ for odd values of J. Concerning the electronic wavefunction ψ_{el}, its general symmetry properties are beyond the scope of this paper. As we limit our interest to the electronic states labelled as Σ^+ it is enough to quote the textbook result that for such states ψ_{el} remains unaltered when inverted about the origin; for further details we refer a curious reader to the literature (see e.g. [4]). Two fundamental selection rules specify the allowed electric dipole transitions between molecular levels: $\Delta J = 0, \pm 1$, mentioned in section 3.1, and $+ \leftrightarrow -$ (the latter reflects the fact that the electric dipole moment operator changes its sign upon inversion).

For the B $\rightarrow$ X transition under consideration, the symmetry properties of the rotational levels for the X $^1\Sigma_g^+$ and B $^1\Sigma_u^+$ states follow from the above considerations and are shown in figure 5. Taking into account the selection rules on symmetry and J, only the P and R branches are allowed. The $+ \not\leftrightarrow +$ and $- \not\leftrightarrow -$ selection rules automatically rule out the Q branch ($\Delta J = 0$).

Appendix II

The frequency of molecular rotation can be determined from the following consideration. According to quantum mechanics, the angular momentum M of the molecule can have only discrete values

$$M = \frac{h}{2\pi}\sqrt{J(J+1)} \qquad (J = 0, 1, 2 \ldots). \qquad \text{(AII.1)}$$

On the other hand, as in classical mechanics

$$M = 2\pi f_{\mathrm{rot}} I = 2\pi f_{\mathrm{rot}} \mu R_{\mathrm{e}}^2. \quad \text{(AII.2)}$$

From comparison of both formulae (using the rotational constant $B = h/8\pi^2 c\mu R_{\mathrm{e}}^2$) we get

$$f_{\mathrm{rot}} = 2cB\sqrt{J(J+1)}. \quad \text{(AII.3)}$$

Appendix III

The wavefunctions of harmonic oscillator are given by [4]

$$\psi_{\mathrm{vib}}(v) = N_v \exp(-1/2\alpha x^2) H_v(\sqrt{\alpha}x). \quad \text{(AIII.1)}$$

Here

$$N_v = \sqrt{\frac{1}{2^v v!}\sqrt{\frac{\alpha}{\pi}}}$$

is a normalization factor, $\alpha = 4\pi^2\mu c\omega_{\mathrm{e}}/h$ and $x = R - R_{\mathrm{e}}$ denotes displacement of the nuclei from their equilibrium distance. $H_v(z)$ are Hermite polynomials of the vth degree. Their explicit form can be easily derived from the recursive formula [12]

$$H_{v+1}(z) = 2zH_v(z) - 2vH_{v-1}(z) \quad \text{(AIII.2)}$$

with $H_0(z) = 1$ and $H_1(z) = 2z$.

Appendix IV

Even if we neglect weak influence of nuclear spins on molecular energy levels (the so-called hyperfine structure), they can considerably affect molecular spectra. The reason lies again in the symmetry properties of molecular levels. In a homonuclear diatomic molecule in which both nuclei are the same isotope the total wavefunction of the molecule ψ_{total} must be symmetrical with respect to exchange of the two nuclei if the nuclear spins are integral $(0, 1, 2\ldots$—boson nuclei). For half-integral nuclear spins $(1/2, 3/2, \ldots$—fermion nuclei) ψ_{total} must be antisymmetrical. Again, each of the four factors in the total molecular wavefunction (AI.1) has well-defined symmetry properties under nuclear exchange. A detailed discussion can be found in the literature [4–7]. In particular, for the B $^1\Sigma_{\mathrm{u}}^+$ state of I_2, ψ_{el} changes to $-\psi_{\mathrm{el}}$ (note that the electronic wavefunction depends also on nuclear coordinates!). The vibrational wavefunction ψ_{vib} is always unaffected by exchange of the nuclei since it depends only on $|\boldsymbol{R}|$. The rotational part ψ_{rot} is symmetrical for even values of J but changes to $-\psi_{\mathrm{rot}}$ for odd J values. The symmetry of the nuclear wavefunction ψ_{nucl} depends on the mutual orientation of two nuclear spins; both symmetrical and antisymmetrical ψ_{nucl} are possible for a given molecule, but not at the same time. Moreover, since the probability of a reorientation of nuclear spins is extremely small (in the absence of magnetic fields and catalytic agents the mean lifetime for such orientation may be of order of months [4]), a molecule with, say, symmetrical ψ_{nucl} will remain in this state practically forever. As a result molecular gas can be regarded as combination of two components: the ortho molecules with symmetrical ψ_{nucl} and the para molecules with antisymmetrical ψ_{nucl}, which stay alongside without mixing with each other. To maintain a required symmetry of ψ_{total}, each modification corresponds either to even or to odd J values.

In the particular case of our experiment, the rules quoted above show that the coordinate part of the molecular wavefunction for the B state ($v' = 11, J' = 128$) level is antisymmetrical with respect to exchange of the nuclei. Since the nuclear spin of iodine is 5/2 [10], ψ_{total} must be antisymmetrical. Therefore only ortho molecules are excited by the laser radiation (figure 5). The collisional transfer can proceed exclusively within the ortho modification and therefore collisions carry the molecule from the level $J' = 128$ only to other even J' levels. As the probability of inelastic collisional transfer between two levels falls rapidly with their increasing energy mismatch, the $J' = 126$ and $J' = 130$ levels are primarily populated.

References

[1] D'Alterio R, Mattson R and Harris R 1974 *J. Chem. Educ.* **51** 282
[2] George S and Krishnamurthy N 1989 *Am. J. Phys.* **57** 850
[3] Lewis E L, Palmer C W P and Cruickshank J L 1994 *Am. J. Phys.* **62** 350
[4] Herzberg G 1950 *Molecular Spectra and Molecular Structure* (Princeton, NJ: Van Nostrand)
[5] Steinfeld J I 1975 *Molecules and Radiation* (New York: Harper & Row)
[6] Dunford H B 1968 *Elements of Diatomic Molecular Spectra* (Reading, MA: Addison-Wesley)
[7] Struve W S 1989 *Fundamentals of Molecular Spectroscopy* (New York: Wiley)
[8] Sakurai K and Broida H 1970 *J. Chem. Phys.* **53** 1615
[9] Gerstenkorn S and Luc P 1985 *J. Physique (Paris)* **46** 867
[10] Radzig A A and Smirnov B M 1985 *Reference Data on Atoms, Molecules and Ions* (Berlin: Springer)
[11] Wood R W and Loomis F 1928 *Phil. Mag.* **6** 231
[12] Korn G A and Korn T M 1968 *Mathematical Handbook for Scientists and Engineers* (New York: McGraw-Hill)

Extending the Diatomic FTIR Experiment: A Computational Exercise To Calculate Potential Energy Curves

Osman Sorkhabi,* William M. Jackson, and Iraj Daizadeh*
Department of Chemistry, University of California, Davis, CA 95616

A standard experiment in undergraduate physical chemistry courses is the ro-vibrational study of diatomics or other small molecules (*1–3*). The ultimate aim of these experiments is to develop an understanding of how to obtain molecular constants from an observed spectrum. These constants allow for the generation of potential energy curves or for calculation of spectra. The potential energy curves are related to the forces that govern the interaction between individual nuclei, and the calculated spectra provide insight into the population of states and their corresponding energies.

Here we propose an experiment for undergraduate physical chemistry courses for calculating potential energy curves for a series of diatomic molecules using the Morse function (*1–3*), a modified Morse function also known as the Hulburt–Hirschfelder (HH) function (*4*), and the Rydberg–Klein–Rees (RKR) (*5*) method from the experimentally determined molecular constants or from fundamental frequencies. This exercise will serve as an extension to the standard IR absorption experiments and will tie together experimental and computational techniques, providing students with a more complete picture of the system under study. Furthermore, this exercise will not only give students a better understanding of the fundamental concepts of spectroscopy and quantum mechanics, but it will also expose them to computational methods. The use of a computer code (Basic, Fortran, C, etc.) and/or a spreadsheet software is encouraged in this project.

Potential Energy Curves

For a diatomic molecule, one can construct a potential energy curve by using the Morse function, which can be written as

$$V_M(x) = D_e[1 - e^{-ax}]^2 \tag{1}$$

where D_e is the depth of the well and is known as the dissociation energy of the molecule, $x = r - r_e$, and r_e is the equilibrium internuclear separation. The constant a gives a measure of the curvature of the function and is given by

$$a = \omega_e\left(\frac{2\pi^2 c\mu}{D_e h}\right)^{1/2} \tag{2}$$

where μ is the reduced mass, ω_e is the fundamental frequency, and c and h are the speed of light and Planck's constant, respectively. Substitution of the Morse function into the time-independent Schrödinger wave equation yields vibrational energy levels in better agreement with experiment than the harmonic oscillator predictions. Equation 1 is not, however, accurate in the sense that it fails to approach D_e rapidly enough. Hulburt and Hirschfelder (*4*) have suggested the following modification to the Morse function:

$$V_{HH}(x) = D_e[(1 - e^{-ax})^2(1 + abx)] \tag{3}$$

Here, a is as defined by eq 2, and b and c as follows:

$$c = 1 - \frac{1}{a r_e}\left(1 - \frac{\alpha_e \omega_e}{6B_e^2}\right) \tag{4}$$

$$b = 2 - \frac{1}{c}\left[\frac{7}{12} - \frac{1}{a^2 r_e^2}\left(\frac{5}{4} + \frac{5\alpha_e\omega_e}{12B_e^2} + \frac{5\alpha_e^2\omega_e^2}{144B_e^4} + \frac{2\omega_e x_e}{3B_e}\right)\right] \tag{5}$$

α_e is the rotational-vibrational interaction constant, and B_e is the rotational constant. Note that c and b are unitless and that c in eqs 4 and 5 is not the speed of light. To obtain eqs 3–5, we modified the expressions found in refs *4* and *9*.[1] Using eqs 4 and 5, we were able to generate c and b for several diatomic molecules. The results are shown in Table 1 along with some other molecular constants. It should be noted that many discrepancies were found between data reported in ref *4* and our calculated values for c and b.

Using the data in Table 1 along with eqs 1–5, one can calculate the Morse function, $V_M(x)$, and the Hulburt–Hirschfelder function, $V_{HH}(x)$, over the full range of r for the given diatomic molecules. However, the above calculations need not be limited to these particular molecules. Any diatomic molecule for which the molecular constants are available can be subject to this type of analysis. A plot of $V_M(x)$ or $V_{HH}(x)$ versus r constitutes a potential energy curve for that particular molecule.

Both the Morse and the Hulburt–Hirschfelder methods assume an analytical, yet empirical, expression for the potential energy function. In contrast to this, a method formulated by Rydberg and Klein allows one to construct the potential energy curve for any diatomic molecule, point for point, from its molecular constants or fundamental frequencies (*7–9*).

The Rydberg–Klein method involves calculating classical turning points as a function of total energy U until the entire potential energy curve is constructed. When U is less than or equal to the potential energy, V_∞, the displacement from the equilibrium bond length, r_e, will be confined to a region between r_- and r_+, where

$$r_+ = \left(\frac{f}{g} + f^2\right)^{1/2} + f \tag{6}$$

$$r_- = \left(\frac{f}{g} + f^2\right)^{1/2} - f \tag{7}$$

Here, f and g are defined as

$$f = \left(\frac{h}{8\pi^2 c\mu\omega_e x_e}\right)^{1/2} \ln(Q) \tag{8}$$

*Corresponding authors.

Table 1. Molecular Constants and Calculated Values for *c* and *b* for Some Diatomic Molecules

Molecule	ω_e (cm^{-1})	$\omega_e x_e$ (cm^{-1})	B_e (cm^{-1})	α_e (cm^{-1})	r_e (Å)	D_e (cm^{-1})	*c*	*b*
N_2	2359.61	14.445	2.007	0.018	1.095	60,738	0.1840	1.070
$H^{79}Br$	2649.67	45.21	8.471	0.226	1.414	31,674	0.0653	1.466
$D^{35}Cl$	2145.163	27.1825	5.4488	0.11329	1.2746	36,142	–[a]	–[a]
NO	1906.52	14.504	1.709	0.0183	1.150	43,644	0.1430	1.092
CO	2168.2	13.04	1.9310	0.01744	1.1284	74,840	0.0567	1.568

[a] Values of *c* and *b* for $D^{35}Cl$ are not known, nor were they calculated.

$$g=\left(\frac{2\pi^2 c\mu}{h\left(\omega_e x_e\right)^3}\right)^{1/2}\left[\alpha_e\left(4\omega_e x_e U\right)^{1/2}+\left(2\omega_e x_e B_e-\alpha_e\omega_e\right)\ln\left(Q\right)\right] \quad (9)$$

where

$$Q=\left\{\frac{\left(w_e^2-4\omega_e x_e \underline{U}\right)^{1/2}}{w_e-\left(4\omega_e x_e \underline{U}\right)^{1/2}}\right\}$$

Equations 8 and 9 are the analytical solutions obtained by Rees for a quadratic in v (*5*) (and thus called second-order RKR). With eqs 6–9, the classical turning points can be calculated over a large range of $\underline{U}$. For the RKR method, $\underline{U}$ need not be quantized and can take on any positive value. A plot of $\underline{U}$ versus r_+ and r_- yields the potential energy curve.

Results of Calculations

Figure 1 shows the IR absorption spectrum of HCl recorded on a Mattson Galaxy Series FTIR 3000 spectrometer with a resolution of 0.1 cm^{-1}. Owing to the high resolution of this spectrometer, transitions due to $H^{35}Cl$ and $H^{37}Cl$ are resolved and can be seen in Figure 1. We also observed transitions due to $D^{35}Cl$ and $D^{37}Cl$, but these are not shown here. In the following analysis, we restrict our attention to $H^{35}Cl$. From the spectrum shown in Figure 1 we have extracted line positions, ν_P and ν_R, and frequency differences, $\Delta\nu(m)$, for the P ($\Delta J = -1$) and R ($\Delta J = +1$) branches, respectively. Using these line positions along with $\Delta\nu(m)$'s, one can calculate ω_e, B_e, and α_e for HCl as follows. The energies for the R and P branches are

$$\nu_R=\nu_0+(2B_e-3\alpha_e)+(2B_e-4\alpha_e)J''-\alpha_e J''^2 \quad J''=0,1,2,\ldots$$

$$\nu_P=\nu_0-(2B_e-2\alpha_e)J''-\alpha_e J''^2 \quad J''=1,2,3,\ldots$$

respectively, where ν_0, the frequency for the forbidden transition from $v''=0, J''=0$ to $v'=1, J'=0$, is given by $\nu_0=\omega_e-2\omega_e x_e$. Now, if we make the substitutions $m_R = J'' + 1$ for the R branch and $m_P = -J''$ for the P branch, the frequency between adjacent lines becomes

$$\Delta\nu(m_i)=\nu(m_i+1)-\nu(m_i)=(2B_e-3\alpha_e)-2\alpha_e m_i \quad (13)$$

where $i = R$ or P. The values of B_e and α_e can be determined by plotting $\Delta\nu(m_i)$ versus m_i. Table 2 lists calculated values for ν_P, ν_R, $\Delta\nu_P$, $\Delta\nu_R$ for $J'' = 0$ to 12 obtained from Figure 1. One can also obtain the value of ν_0 and ω_e using the above equations, provided that $\omega_e x_e$ is known. This is not the most common or accurate computational method for fitting molecular constants, but we used this approach because of its simplicity. The reader is referred to ref *11* for further information on different techniques of fitting molecular constants. For reference, we have calculated values for ω_e, α_e, and B_e from the spectrum and they appear, along with literature values (*9*), in Table 3.

Using our calculated molecular constants, we have constructed potential energy curves for HCl using the Morse, HH, and RKR methods as shown in Figure 2. Using data near the potential energy minimum to generate the entire

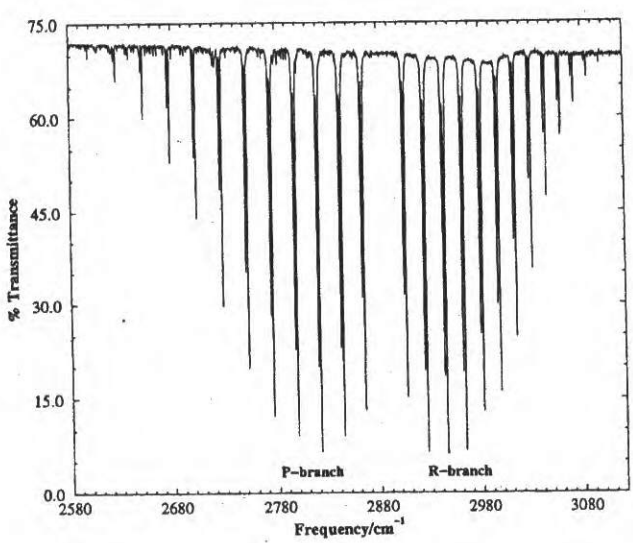

Figure 1. FTIR ro-vibrational spectrum of HCl. Notice that the isotope effect can be seen.

Table 2. Measured Line Positions (ν) and Frequency Differences (Δν) for P and R Branches of $H^{35}Cl$

$J\leq$	m_P	$\Delta\nu_P$	ν_P (cm^{-1})	m_R	$\Delta\nu_R$	ν_R (cm^{-1})
0	0	–	–	1	–	2905.95
1	-1	–	2864.97	2	19.77	2925.72
2	-2	21.45	2843.52	3	19.04	2944.76
3	-3	22.18	2821.34	4	18.32	2963.08
4	-4	22.66	2798.68	5	17.84	2980.92
5	-5	23.14	2775.54	6	16.88	2997.8
6	-6	23.62	2751.92	7	16.39	3014.19
7	-7	24.35	2727.57	8	15.67	3029.86
8	-8	24.83	2702.74	9	14.94	3044.8
9	-9	25.07	2677.67	10	14.23	3059.03
10	-10	25.79	2651.88	11	13.74	3072.77
11	-11	26.28	2625.6	12	12.77	3085.54
12	-12	26.75	2598.85	13	12.05	3097.59

Table 3. Calculated Data for $H^{35}Cl$

Term[a]	This Work[b]	Lit. Value[c] (9)
ω_e (cm^{-1})	2989.74 ± 0.23	2990.946
α_e (cm^{-1})	0.288 ± 0.004	0.30718
B_e (cm^{-1})	10.55 ± 0.04	10.59341
$\omega_e x_e$ (cm^{-1})	–	52.8186
c	0.0399	0.0163
b	1.765	4.9090

[a] The molecular constants are for the naturally abundant species, not for isotopic averages.
[b] Errors represent the 95% confidence interval.
[c] Values for c and b were calculated using the molecular constants reported in ref 9.

potential energy curve will unavoidably introduce error due to the function becoming more and more approximate at points far from the equilibrium bond distance. In a future study, we will explicitly address this issue by doing overtone IR experiments to get the necessary molecular parameters. Nonetheless, all three methods resemble, very accurately, the "true" potential energy curve near r_e. The Morse curve, however, approaches the asymptotic limit, D_e, slower that the HH energy curve. The dissociation energy predicted by the RKR method given above can be written as

$$D_e = \frac{\omega_e^2}{4\omega_e x_e} \qquad (14)$$

Using this expression for D_e, the Morse and the RKR methods are mathematically equivalent using second-order RKR. However, eq 14 does not yield the true dissociation energy and was not used in any of the our calculations. One more point should be made regarding the results of the RKR method. Equations 8 and 9 fail to improve on the results of the Morse potential energy curve because it is a quadratic solution. More accurate results can be obtained by using more sophisticated solutions of the Rydberg–Klein formulation (*5*, *13*). Finally, we would like to mention that these methods are not limited to ground electronic states but can be applied to excited states as well.

Conclusions

To our knowledge, no other experiment incorporates calculations of potential energy curves. The uniqueness of this approach is that it ties computational techniques with a standard physical chemistry experiment. We believe that extending the IR HCl experiment will allow students to relate theory to experiment and gain greater insight into the system under study.

The above exercise was assigned as a final project to an upper division undergraduate class entitled Molecular Structure and Spectroscopy at the University of California–Davis campus. The students were asked to:

- calculate molecular constants from experimentally obtained spectra,
- compare these values with literature, and
- generate potential energy curves for the given diatomic molecule using the Morse, HH, and RKR methods.

The class performed the calculations both from spreadsheet software and using a C code.[2] The results were very encouraging. However, since the dissociation energy can be defined by eq 14, the students seemed perplexed as to why the Morse and the RKR quadratic formulation gave the same result. Overall, students performed very well on this project and with enthusiasm.

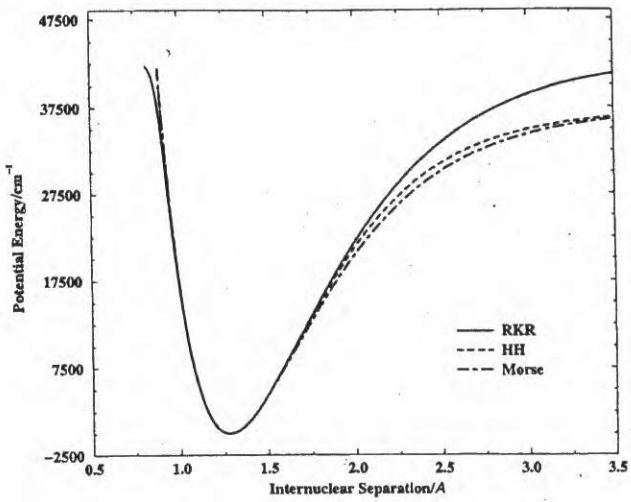

Figure 2. Potential energy curve from the observed band-spectroscopic data for HCl using the Rydberg–Klein–Rees, Morse, and Hulburt–Hirschfelder methods.

Acknowledgments

Iraj Daizadeh gratefully acknowledges the support of A. A. Stuchebrukhov. We are grateful for the helpful comments of W. H. Fink and fellow graduate student J. Wrobel, who was a teaching assistant to the course. We are also thankful to the Chemistry Department staff at the University of California for providing the HCl sample and the allowed time on the departmental FTIR instrument.

Notes

1. A mistake was found for eq 5 from the original refs *4* and *11*. This error was addressed in an erratum presented in ref *14*.
2. The C code used can be obtained from I. Daizadeh via email: *daizadeh@indigo.ucdavis.edu*.

Literature Cited

1. Shoemaker, D. P.; Garland, C. W.; Nibler, J. W. *Experiments in Physical Chemistry*, 5th ed.; McGraw-Hill: New York, 1989.
2. Hollas, J. M. *Modern Spectroscopy*; Wiley: New York, 1987.
3. Atkins, P. W. *Physical Chemistry*, 5th ed.; Freeman: New York, 1994.
4. Hulburt, H. M.; Hirschfelder, J. O. *J. Chem. Phys.* **1941**, *9*, 61.
5. Rees, A. L. G. *Proc. Phys. Soc. London* **1947**, *59*, 998–1008.
7. Klein, O. *Z. Physik* **1932**, *76*, 226.
8. Rydberg, R. *Z. Physik* **1932**, *73*, 376.
9. Rydberg, R. *Z. Physik* **1933**, *80*, 514.
10. Graybeal, J. D. *Molecular Spectroscopy*, Rev. 1st ed.; McGraw-Hill: New York, 1988; pp 332–333.
11. Herzberg, G. *Molecular Spectra and Molecular Structure I. Spectra of Diatomic Molecules*, 2nd ed.; Van Nostrand: New York, 1950.
12. Schor, H. H. H.; Teixeira, E. L. *J. Chem. Educ.* **1994**, *71*, 771.
13. Senn, P. *Computers Chem.* **1995**, *19*, 437.
14. Hulburt, H. M.; Hirschfelder, J. O. *J. Chem. Phys.* **1961**, 1901.

J. Physique 46 (1985) 867-881 JUIN 1985, PAGE 867

Classification
Physics Abstracts
33.20K — 31.90

Description of the absorption spectrum of iodine recorded by means of Fourier Transform Spectroscopy : the (B-X) system

S. Gerstenkorn and P. Luc

Laboratoire Aimé Cotton (*), C.N.R.S. II, Bâtiment 505, 91405 Orsay Cedex, France

(*Reçu le 3 décembre 1984, accepté le 6 février 1985*)

Résumé. — L'analyse de la totalité du spectre d'absorption de la molécule d'iode représenté par le système (B-X) I_2 et enregistré par spectroscopie par transformation de Fourier est présentée. On montre que les 100 000 transitions enregistrées et publiées dans plusieurs Atlas peuvent être recalculées au moyen de 46 constantes : 45 étant les coefficients de Dunham servant à décrire les constantes vibrationnelles et rotationnelles des états X jusqu'à $v'' = 19$ et de l'état B jusqu'à $v' = 80$ (niveau situé à 1,6 cm^{-1} de la limite de dissociation), plus un coefficient empirique permettant de tenir compte des constantes de distorsions négligées (supérieures à M_v). L'erreur quadratique moyenne entre les nombres d'ondes recalculés et mesurés est trouvée égale à 0,002 cm^{-1} en accord avec la comparaison des écarts entre les nombres d'ondes recalculés et les nombres d'ondes absolus de nombreuses raies de l'iode mesurées indépendamment.

Abstract. — An *in extenso* analysis of the (B-X) I_2 iodine absorption spectrum recorded by means of Fourier Transform Spectroscopy is presented. It is shown that the 100 000 recorded transitions covering the 11 000-20 040 cm^{-1} range and published in several Atlases may be recalculated by means of only 46 constants : 45 are Dunham coefficients describing the vibrational and rotational constants of both X state (up to $v'' = 19$) and B state (up to $v' = 80$, situated only at 1.6 cm^{-1} from the dissociation limit of the B state), and one empirical scaling factor which takes account of neglected centrifugal constants higher than M_v. The overall standard error between computed and measured wavenumbers is equal to 0.002 cm^{-1} in agreement with the differences of numerous independent absolute wavenumbers and the computed ones.

1. Introduction.

1.1 HISTORICAL. — First, let us recall that the study of the absorption spectrum of iodine by means of Fourier Transform Spectroscopy (F.T.S.) was undertaken at Aimé Cotton Laboratory, seven years ago, in 1977. At that time, the aim of the work was to test the performances of F.T.S. in the visible range (where the multiplex gain is lost) and to show that F.T.S. remains an excellent tool for emission and absorption studies [1-3], even in cases where the noise is mainly due to the signal itself (photon noise). We concluded our study by the following statement [4] :

« The method (F.T.S.) can be expected to open not only significant new spectroscopic experiments but it also allows a complete high-precision remeasurement of the existing molecular spectra in the visible and U.V. (electronic vibrational transitions). » As usual, we were not prophets in our country, and we have felt that the analysis of only a few bands [3, 4] of iodine was not enough to assess the above statement. Thus, we published also an « Iodine Atlas », encompassing a large spectral range from 14 800 to 20 000 cm^{-1} [5b] (note that this atlas was not the first one : Simmons and Hougen, using conventional grating spectroscopy, have published a short time before an « iodine atlas » covering the 18 000-19 000 cm^{-1} range [6]). However, a spectrum, beautiful though it may be, remains solely a collection of numbers, until its complete analysis is achieved. Analysis of the iodine absorption spectrum was a challenge for us, because numerous, extended and careful studies of the (B-X) system were already made at this time [7-11].

Nevertheless, in the fundamental paper published by Barrow and Yee [7], one point remains unexplained : their experimental vibrational constants $G(v)$ do not follow, at least above $v' = 50$, the classical Dunham expression $G(v) = \sum_{n=1} y_{n0}(v + 1/2)^n$. The origin of this difficulty may be either the existence of a

(*) Laboratoire associé à l'Université Paris-Sud.

in the present case [19]. For inclusion in the least squares fits the CDC values belonging to the B state for $0 \leqslant v' \leqslant 80$, were represented by exponential polynomials and noted « CDC_s » :

$$D_v = \exp \sum_{i=1} C_{di}(v + 1/2)^{i-1}$$

$$- H_v = \exp \sum_{i=1} C_{hi}(v + 1/2)^{i-1}$$

$$- L_v = \exp \sum_{i=1} C_{li}(v + 1/2)^{i-1}$$

$$- M_v = \exp \sum_{i=1} C_{mi}(v + 1/2)^{i-1}$$

obtained from fits of the calculated values according to Hutson's method. Only exponentials provide an adequate representation of the calculated CDC values, without loss of precision. Indeed these constants increase rapidly at high v and finally diverge at dissociation [37].

The vibrational and rotational constants (as well as the CDC of the ground state up to $v'' = 19$) are accurately represented by the classical Dunham expansion series [38]

$\sum y_{il}(v + 1/2)^i$, where

$\begin{cases} l = 0 \text{ and } i = 1, 2, \ldots i \text{ for } G_v \\ l = 1, 2, 3, \ldots \text{ and } i = 0, 1, 2, \ldots i \text{ for } B_v, D_v, H_v . \end{cases}$

The input data of the least squares fit are the 17 800 measured wavenumbers which obey equation (3) or (4). (These equations are derived from Eqs. (1) and (2), $\sigma_R(J)$ for $\Delta J = -1$ and $\sigma_P(J)$ for $\Delta J = +1$.)

$$\sigma_R(J) = T_e + G_{v'} + B_{v'} \alpha + \\ + [- D_{v'} \alpha^2 + H_{v'} \alpha^3 + L_{v'} \alpha^4 + M_{v'} \alpha^5] \\ - (G_{v''} + B_{v''} \gamma - D_{v''} \gamma^2 + H_{v''} \gamma^3) \quad (3)$$

$$\sigma_P(J) = T_e + G_{v'} + B_{v'} \alpha + \\ + [- D_{v'} \beta^2 + H_{v'} \beta^3 + L_{v'} \beta^4 + M_{v'} \beta^5] \\ - (G_{v''} + B_{v''} \gamma - D_{v''} \gamma^2 + H_{v''} \gamma^3) \quad (4)$$

(where $\alpha = (J + 1)(J + 2)$, $\gamma = J(J - 1)$, $\beta = J \times (J - 1)$ and $T_e = T_{0,0} + G''_0 - G'_0$; $T_{0,0}$ being the distance between the ground level $v'' = 0, J = 0$ of the X state and the level $v' = 0, J = 0$ of the B state), the unknowns being the molecular constants. If the CDC values of the B state are known from theory, the centrifugal distortion contribution (quantities in brackets, Eqs. (3) and (4)) can be subtracted from the « raw » measured wavenumbers $\sigma_R(J)$ and $\sigma_P(J)$ leading to « distortion-free » wavenumbers. A further simplification of the system is obtained by assuming that the ground state's constants are well known and are equal to those deduced from the IPA potential (Table III). Finally it remains to fit a system containing 17 800 corrected wavenumbers to an expression with 162 unknowns : the 81 vibrational $G_{v'}$ constants and the 81 rotational constants $B_{v'}$ belonging to the B state with $0 \leqslant v' \leqslant 80$. The principal problem consists of determining good initial $G_{v'}$ and $B_{v'}$ values in order to start the iterative procedure (Fig. 4). For this purpose a preliminary least squares fit is made with the raw measured wavenumbers where only the molecular constants $G_{v'}$, $B_{v'}$, $D_{v'}$ and $H_{v'}$ are taken into account. The centrifugal distortion constants $L_{v'}$ and $M_{v'}$ are too small for empirical determination, hence they were set to be equal to zero in the preliminary fit.

Once a set of $G_{v'}$ and $B_{v'}$ constants are known, their Dunham expansion parameters are determined and a RKR [39] curve may be constructed [40] and used to generate centrifugal distortion constants [19, 41]. An iterative approach is then necessary to obtain a self-consistent set of vibrational, rotational and centrifugal distortion constants [9, 19].

However transitions connected to rotational levels with high J values (levels situated between the two full lines $- M_v K^5 = 0.001$ cm^{-1} and $- M_v K^5 = 0.025$ cm^{-1} ($K = J(J + 1)$ in Fig. 5) require distortion constants higher than $M_{v'}$ in order to be accurately recalculated). By means of effective $M_v^* = kM_v$ constants, which take account of the neglected higher N_v, O_v... constants (see Ref. [20]), and where k is an empirical scaling factor equal to 2.2, it was possible to handle the whole field of data (Table I and Figs. 5 and 6) in one sweep.

Including the $M_v^* = kM_v$ effective constants in the fits, the procedure represented by figure 4 converges rapidly and only two iterations were required. The resulting overall standard error $\hat{\sigma}$ between the 17 800 computed wavenumbers and the measured ones was 0.002 cm^{-1}. The least squares fits were unweighted

Table III. — *Dunham coefficients describing the vibrational and rotational molecular constants of the* B *state (valid up to* $v' = 80$*) and* X *state (valid up to* $v'' = 19$*). The number of significant digits necessary to recalculate the wavenumbers of the transition belonging to the* (B-X) I_2 *system is given in parentheses :* $y_{i0}(12)$, $y_{i1}(11)$.

X state $0 \leqslant v'' \leqslant 19$

i	y_{i0}	i	y_{i1}
1	0.2145292253831637D+03	0	0.3736812559337480D-01
2	-.6129731614337341D+00	1	-.1138151197256179D-03
3	-.1027340004155040D-03	2	-.3061638399475614D-06
4	-.1427228811574466D-03	3	-.4093271255246214D-08
5	0.8765347546885206D-05	4	0.9542617587865405D-10
6	-.3036676438177481D-06	5	-.4664721586567808D-11
7	0.4241664120510493D-08		

B state $0 \leqslant v' \leqslant 80$

i	y_{i0}	i	y_{i1}
1	0.1256686951781 3D+03	0	0.2900072710830-01
2	-.7503998360394 8D+00	1	-.1494374068110-03
3	-.4144041450207 3D-02	2	-.1260399161870-05
4	0.2248931158086 4D-03	3	0.3608438524040-07
5	-.3228682530208 2D-04	4	-.1189367647840-07
6	0.2827402678223 1D-05	5	0.1608364607590-08
7	-.1697605952591 2D-06	6	-.1401499215720-09
8	0.7248339198431 4D-08	7	0.8170822731460-11
9	-.2236683436162 1D-09	8	-.3295261010210-12
10	0.5024159532913 0D-11	9	0.9372593161760-14
11	-.8183150076487 4D-13	10	-.1892810670610-15
12	0.9520574918516 4D-15	11	0.2698752289210-17
13	-.7683789243394 7D-17	12	-.2657234093550-19
14	0.4075803322639 1D-19	13	0.1720321435180-21
15	-.1275286930700 5D-21	14	-.6592904440780-24
16	0.1780620741121 1D-24	15	0.1133496022970-26